Mon. Not. R. Astron. Soc. **000**, 1–6 (2008) Printed 6 September 2011 (MN LaTeX style file v2.2)

Constraints on magnetic field strength in the remnant SN 1006 from its nonthermal images

O. Petruk[1,2], T. Kuzyo[2], F. Bocchino[3]
[1] *Institute for Applied Problems in Mechanics and Mathematics, Naukova St. 3-b, 79060 Lviv, Ukraine*
[2] *Astronomical Observatory, National University, Kyryla and Methodia St. 8, 79008 Lviv, Ukraine*
[3] *INAF Osservatorio Astronomico di Palermo, Piazza del Parlamento 1, 90134 Palermo, Italy*

arXiv:1109.0831v1 [astro-ph.HE] 5 Sep 2011

Accepted .... Received ...; in original form ...

ABSTRACT

Images of SN 1006 have a number of important properties. For instance, the bright limbs coincide spatially in various bands, they have different brightness, and the contrast of brightness varies from radio to gamma-rays. The reasons of such properties and the role of the magnetic field strength are discussed. Simple, almost model-independent methods and analytical approximations for the derivation of the strength of magnetic field from the comparison of radio, X-rays and TeV images of SNR are presented. The methods require the TeV image to be well resolved and accurate, at least to the level of the radio and X-ray maps, in order to put reasonable constraints on magnetic field. If we apply it to the present HESS data, they limit the strength of magnetic field in limbs of SN 1006 to values lower than few hundreds micro Gauss. If applied to the Fermi-LAT band, the model predicts same position and same ratio of the surface brightness for GeV photons as for the radio band. We conclude that TeV and GeV future high-resolution data may be very informative about the MF of SN 1006.

Key words: ISM: supernova remnants – individual:SN 1006 – ISM: cosmic rays – radiation mechanisms: non-thermal – acceleration of particles

1 INTRODUCTION

Supernova remnant (SNR) SN 1006 is one of the most interesting objects for studies of Galactic cosmic rays. It is quite symmetrical with rather simple bilateral morphology in radio (e.g. Petruk et al. 2009a), nonthermal X-rays (e.g Miceli et al. 2009) and TeV γ-rays (Acero et al. 2010). Its prominent feature is the positional coincidence of the two bright nonthermal limbs in all these bands, including TeV γ-rays.

Could such coincidence be sign for leptonic origin of the TeV emission? Detailed numerical modeling reveals factors determining the formation of the patterns of radio, X-ray and γ-ray maps of SNRs (Petruk et al. 2009a,b, 2011a). TeV γ-ray emissivity does not directly depend on the magnetic field (MF) strength B. However, in the regions with the larger post-shock magnetic field, the radiative losses of relativistic electrons are higher. Therefore, their distribution downstream of the shock have to be steeper and the IC emission should be lower. In contrast, X-ray brightness increases in regions with higher MF because emissivity is proportional to $B^{3/2}$. Thus, the coincidence of the TeV γ-limbs with X-ray and radio limbs may not be directly considered as confirmation of the leptonic nature of γ-rays in SNR. Nevertheless, the azimuthal variation of brightness depends not only on the azimuthal variation of MF, but also on the azimuthal dependences of the injection efficiency (fraction of density of accelerated particles) and of their maximum energy, that, under some configurations, can provide correlation of the non-thermal brightness in different bands (Petruk et al. 2009b, 2011a).

In order to check whether the observed correlation of the γ-ray and X-ray brightness may be considered as argument in favor of the IC mechanism of TeV γ-ray emission in SN 1006, a model-independent approach is developed in Petruk et al. (2009c). It bases on the idea that the radio and hard X-ray data contain information about variations of the fraction of density and of the maximum energy of accelerated electrons. The radio and X-ray observations, used with a number of reliable assumptions about MF distribution, are used in Petruk et al. (2009c) to generate image of SN 1006 it should have in TeV γ-rays and to compare it with observations. It is shown that the pattern of the IC image of SN 1006 is naturally similar to its radio and X-ray maps, in various MF configurations. This is a new argument in favor of the leptonic origin of γ-rays from SN 1006.

The further important property of SN 1006 is that the two bright limbs have different brightness. In addition, the ratio of brightness of the limbs is different in radio, hard

X-ray and TeV γ-ray bands. In the present note, we demonstrate that location of the γ-ray limbs and the contrast of brightness in various bands depend on the magnetic field strength. Thus, it may be used to put constraints on MF.

We exploit the approach of Petruk et al. (2009c) in an inverse manner. Namely, once the TeV γ-ray map of SN 1006 is known, we use, beside radio and hard X-ray data, properties of the TeV γ-ray image to put constraints on MF.

Namely, in Sect. 2, we present a new simple method to estimate the strength of MF in SNR from contrasts of brightness in nonthermal limbs and apply it to SN 1006. Another realization of the method to constrain MF, from location of the TeV γ-ray limbs, is proposed in Sect. 3. Application of the methods to the GeV γ-ray image is discussed in Sect. 4. Sect. 5 concludes.

Our approach is model-independent in the sense that it is independent from details of CR acceleration and MHD, it does not involve simulations based on theoretical principles, it is free of any assumptions about SNR energy, distance, structure of interstellar medium and interstellar magnetic field etc. The only assumptions we make are the shape of the electron energy spectrum (which is rather general) and that TeV γ-ray emission is dominated by the inverse-Compton process.

2 MAGNETIC FIELD STRENGTH FROM THE RELATIVE BRIGHTNESS OF THE RADIO, X-RAY AND γ-RAY LIMBS

The ratio of brightness between the two bright limbs in SN 1006 varies with frequency. In particular, the NE limb is brighter in X-rays while the SW limb is more prominent in radio (see Figs. 1, 2 or 11 in Petruk et al. 2009c). If the γ-ray emission of SN 1006 is dominated by IC process, then the ratio of the γ-ray brightness of these limbs depends on the strength of MF in SNR.

Let us consider the uniform plasma with the electron distribution consisting of the (variable) power-law plus the (parameterized) exponential cut off

$$N(E) = KE^{-s+\delta s(E)} \exp\left[-\left(E/E_{\max}\right)^{\alpha}\right] \tag{1}$$

where s is the spectral index, K the normalization, $E_{\max}$ the maximum energy, α the broadening parameter. The function $\delta s(E)$ reflects possible concavity of the spectrum as result of the efficient acceleration (e.g. Berezhko & Ellison 1999; Blasi 2002); it increases monotonically from 0 at around $E \simeq m_e c^2 = 0.5\,\mathrm{MeV}$ to ≤ 0.5 for $E \simeq E_{\max} \sim 10\,\mathrm{TeV}$ (e.g. Berezhko & Ellison 1999; Kang et al. 2009). This function produces negligible changes to our results, since it varies very slowly over decades in energy (for details see Appendix A). Therefore, we use $\delta s = 0$ hereafter.

Parameter α regulates the broadening/narrowing of the high-energy end of the electron spectrum. Different models predicts different values for the parameter. In a number of theoretical models the cut off is broader than the pure exponent (see references in Reynolds & Keohane 1999), suggesting $\alpha < 1$. Such broadening seems to be observed in few SNRs, including SN 1006 (Ellison et al. 2000, 2001; Lazendic et al. 2004; Uchiyama et al. 2003). It should be attributed to the physics of acceleration (Petruk 2006), rather than to the effect of superposition of spectra in different conditions along the line of sight (Reynolds 1996). There are also some recent theoretical evidences that the cut-off may be narrower than the pure exponent depending on how strongly the diffusion coefficient depends on the particle momentum (Blasi 2010). In particular, the value $\alpha = 2$ appears in number of numerical and analytical approaches (Zirakashvili & Aharonian 2007; Blasi 2010; Kang & Ryu 2010; Kang 2011) with arguments that such value is relevant to the Bohm diffusion. The time evolution might decrease this α to a value between 1 and 2 (Schure et al. 2010). In the approximations developed below, we allow α to vary from 0.5 to 2.

Synchrotron radio and IC γ-ray (at 1 TeV) emissivities of electrons destributed with Eq. (1) are approximately related as

$$q_{\mathrm{ic}} \propto q_{\mathrm{r}} B^{-(s+1)/2} \exp\left(-\beta_{\mathrm{ic}}\beta_{\alpha\mathrm{ic}}\left(\frac{c_1 B}{\nu_{\mathrm{break}}}\right)^{0.375\beta_{\alpha\mathrm{x}}}\right). \tag{2}$$

where ν_{break} is a critical frequency of the synchrotron radiation of electrons with energy $E_{\max}$ in magnetic field with strength B, $c_1 = 6.26 \times 10^{18}$ cgs,

$$\begin{aligned} \beta_{\mathrm{ic}} &= \begin{cases} 15, & \text{for } 2 \leq s \leq 2.5 \\ 15 + 2(2-s), & \text{for } 1.8 \leq s < 2 \end{cases}, \\ \beta_{\alpha\mathrm{ic}} &= 1.08\alpha^2 - 0.3\alpha + 0.22, \\ \beta_{\alpha\mathrm{x}} &= \alpha(1.24 - 0.24\alpha). \end{aligned} \tag{3}$$

Details are considered in Petruk et al. (2009c) where the value $\alpha = 1$ was adopted (then $\beta_{\alpha\mathrm{ic}} = \beta_{\alpha\mathrm{x}} \equiv 1$). The relation (2) is a generalization of Eq. (11) in Petruk et al. (2009c); it is valid[1] for any value of α from 0.5 to 2.

Let's consider two regions on SNR image[2] with the same strength B (for example, some parts of the two bright limbs in SN 1006) and denote them with the index '1' (NE limb) and index '2' (SW limb). The ratio $\mathcal{R}_{\mathrm{ic}} = q_{\mathrm{ic1}}/q_{\mathrm{ic2}}$ of IC γ-ray brightness (at 1 TeV) of these regions is

$$\begin{aligned} \mathcal{R}_{\mathrm{ic}} \quad &= \quad \mathcal{R}_{\mathrm{r}} \exp\Big(-\beta_{\mathrm{ic}}\beta_{\alpha\mathrm{ic}}\left(c_1 B\right)^{0.375\beta_{\alpha\mathrm{x}}} \\ &\times \quad \left[\frac{1}{\nu_{\mathrm{break1}}^{0.375\beta_{\alpha\mathrm{x}}}} - \frac{1}{\nu_{\mathrm{break2}}^{0.375\beta_{\alpha\mathrm{x}}}}\right]\Big) \end{aligned} \tag{4}$$

where $\mathcal{R}_{\mathrm{r}} = q_{\mathrm{r1}}/q_{\mathrm{r2}}$ is the ratio of the radio brightness. It is apparent from this formula that the ratio of IC brightness between the two bright limbs in SN 1006 really depends on the absolute value of the magnetic field strength.

The radio and X-ray emissivities are approximately related as

$$q_{\mathrm{x}} \propto q_{\mathrm{r}} \exp\left(-\beta_{\mathrm{x}}\left(\frac{\nu_{\mathrm{x}}}{\nu_{\mathrm{break}}}\right)^{0.364\beta_{\alpha\mathrm{x}}}\right) \tag{5}$$

where $\beta_{\mathrm{x}} = 1.46 + 0.15(2-s)$; this relation generalizes Eq. (8) from Petruk et al. (2009c) to α other than unity; its accuracy is comparable to accuracy of (2). Therefore, the ratio of X-ray brightness between the two limbs $\mathcal{R}_{\mathrm{x}} = q_{\mathrm{x1}}/q_{\mathrm{x2}}$ is

---

[1] The maximum error of the approximation (2) is 30% for s from 1.8 to 2.5, α from 0.5 to 2 and values of $E_{\max}$ which provide non-negligible contribution of the spectrum (1) to γ-ray emission at 1 TeV.

[2] These regions have to be rather small to allow for assumption of uniform MF there.

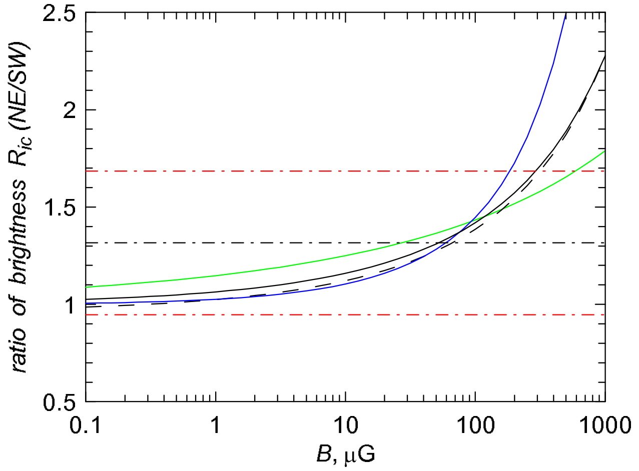

Figure 1. Dependence of the ratio of IC γ-ray brightness $\mathcal{R}_{\rm ic}$ (at 1 TeV) on B, as from Eq. (7) and $\alpha = 1$ (black lines), $\alpha = 0.5$ (green line), $\alpha = 2$ (blue line). The value $s = 2$ is adopted; the plot is however almost insensitive to s. Observed values $\mathcal{R}_{\rm r}$, $\mathcal{R}_{\rm x}$ used for solid lines are obtained from the high-resolution images; those used for dashed line are from the images smoothed to the HESS resolution. Horizontal lines represent the ratio of γ-ray brightness (black) and corresponding 1-σ errors (red) from the data of Acero et al. (2010).

$$\mathcal{R}_{\rm x} = \mathcal{R}_{\rm r} \exp\left(-\beta_{\rm x}\nu_{\rm x}^{0.364\beta_{\alpha{\rm x}}}\left[\frac{1}{\nu_{\rm break1}^{0.364\beta_{\alpha{\rm x}}}} - \frac{1}{\nu_{\rm break2}^{0.364\beta_{\alpha{\rm x}}}}\right]\right). \quad (6)$$

If we neglect differences between the powers 0.364 and 0.375 assuming both equal to 0.37, and substitute (4) with combination in the exponent, consisting of the break frequencies, from (6), we obtain that

$$\mathcal{R}_{\rm ic} \simeq \mathcal{R}_{\rm r}\left(\frac{\mathcal{R}_{\rm x}}{\mathcal{R}_{\rm r}}\right)^{\xi(B)}, \quad \xi = \frac{\beta_{\rm ic}\beta_{\alpha{\rm ic}}(c_1 B)^{0.37\beta_{\alpha{\rm x}}}}{\beta_{\rm x}\nu_{\rm x}^{0.37\beta_{\alpha{\rm x}}}}. \quad (7)$$

This equation relates approximately the ratios of surface brightness between the two regions with the same MF strength (e.g. the bright limbs) in radio, hard X-ray and 1 TeV γ-rays with B as a free parameter. Having $\mathcal{R}_{\rm r}$, $\mathcal{R}_{\rm x}$ and $\mathcal{R}_{\rm ic}$ measured in observations, one may have estimation for the value of MF in these regions. If $s = 1.8 \div 2.2$, $\alpha = 1$ and $\nu_{\rm x} = 2.4\,{\rm keV}$ then $\xi = 0.15B_{\mu}^{0.37}$ where B_{μ} is in μG.

Eq. (7) shows that $\mathcal{R}_{\rm ic}(B)$ is increasing function of B and that in the limit $B \to 0$, the ratio $\mathcal{R}_{\rm ic} \to \mathcal{R}_{\rm r}$.

Let's proceed to the data of observations and consider the radio (VLA+Parkes) image of SN 1006 at 1.5 MHz (Petruk et al. 2009a) as well as its hard X-ray (XMM) image (Miceli et al. 2009). These images have high resolution; for sake of comparison, we will consider also the same radio and X-ray images smoothed to the resolution of HESS (by the Gaussian with $2'$ sigma). The two regions are defined by an annulus ($8'$ to $20'$ from center) centered on the remnant and sectors $27^{\rm o} - 45^{\rm o}$ from north for NE limb and $216^{\rm o} - 234^{\rm o}$ for SW limb. Region are chosen to overlap the maximum in the azimuthal profile of γ-ray brightness and are $18^{\rm o}$ wide that corresponds to one step in the γ-ray profile reported by Acero et al. (2010, their fig. 6).

In SN 1006, $\mathcal{R}_{\rm r} = 0.998$ or 0.958, $\mathcal{R}_{\rm x} = 1.53$ or 1.50 for the high-resolution or the smoothed images respectively. The dependence of the IC brightness ratio $\mathcal{R}_{\rm ic}$ on B calculated with Eq. (7) and these numbers is shown on Fig. 1. One can see that higher MF results in the larger difference between the brightness of the two γ-ray limbs. It is evident that lines obtained from images with the high resolution (solid lines) and from smoothed images (dashed lines) differ just a bit, because regions considered are large enough to be unaffected by the smoothing to few arc minutes. Fig. 1 reveals that the dependences $\mathcal{R}_{\rm ic}(B)$ for various α are similar; though uncertainty in the value of α may result in a bit different estimates of B.

HESS report gives $\mathcal{R}_{\gamma} = 1.32 \pm 0.37$ (Acero et al. 2010, Fig. 2). The later ratio together with errors is shown on Fig. 1 by horizontal lines. Unfortunately, rather slight dependence of the ratio of γ-ray brightness of the value of MF strength (few times versus variation of B over decades) and the large errors in the present HESS data do not allow us to give preference to any strength of MF. Any value between few μG and few hundred μG falls into the 1-σ error. Nevertheless, we believe that the suggested method will be useful in the future when experiments provide increased accuracy and resolution.

3 MF STRENGTH FROM LOCATION OF THE γ-RAY LIMBS

In cases when MF in two regions is different, an approximate formula (7) may be generalized to

$$\mathcal{R}_{\rm ic} \simeq \mathcal{R}_{\rm r}\left(\frac{\mathcal{R}_{\rm x}}{\mathcal{R}_{\rm r}}\right)^{\xi(B_2)} \mathcal{R}_{\rm B}^{-(s+1)/2}$$
$$\times \exp\left(-\beta_{\rm ic}\beta_{\alpha{\rm ic}}\left(\frac{c_1 B_2}{\nu_{\rm break1}}\right)^{0.37\beta_{\alpha{\rm x}}}\left(\mathcal{R}_{\rm B}^{0.37\beta_{\alpha{\rm x}}} - 1\right)\right) \quad (8)$$

where $\mathcal{R}_{\rm B} = B_1/B_2$.

IC γ-ray emission is expected to be smaller where the strength of MF is higher (e.g. Aharonian & Atoyan 1999) while the synchrotron emission $\propto B^{3/2}$. This might result in an γ-ray 'limb-inverse' property for SNRs (Petruk et al. 2009b). Namely, the faintest IC γ-ray regions in SNR images might be located where the radio and X-ray images have maximum brightness. If this would happen in SN 1006, then IC γ-ray limbs would be expected in SE-NW regions, in contrast to radio and X-ray limbs which are at NE-SW azimuths.

Let's now, in contrast to Sect. 2, denote with the indexes '1' and '2' the values in NE bright limb and in SE faint region of SN 1006, respectively. These two regions are separated in azimuth on $90^{\rm o}$, thus MF is expected to differ up to few times there; in particular, in the classic model of MF inside SNR (i.e when ISMF is assumed constant and the only compression of ISMF is considered which depends on the obliquity of the shock), $\mathcal{R}_{\rm B}$ varies from 1 for an aspect angle (between the ambient MF and the line of sight) $\phi_{\rm o} = 0^{\rm o}$ to $\mathcal{R}_{\rm B} = 4$ for $\phi_{\rm o} = 90^{\rm o}$. Therefore, we should use Eq. (8). In this formula, the ratio $\mathcal{R}_{\rm ic}$ could be higher than unity (that corresponds to the observed location of γ-ray limbs in SN 1006) or less than unity (that reflects the inversion of the γ-ray limbs). Eq. (8) shows that the value of $\mathcal{R}_{\rm ic}$ depends, – beside observables s, $\mathcal{R}_{\rm r}$, $\mathcal{R}_{\rm x}$ and $\nu_{\rm break1}$, – on the strength B_2, on contrast $\mathcal{R}_{\rm B}$ and on α. Thus, the observed location of γ-ray limbs can also give constraints on the MF field in SN 1006; namely, on B_2 and $B_1 = \mathcal{R}_{\rm B}B_2$. In

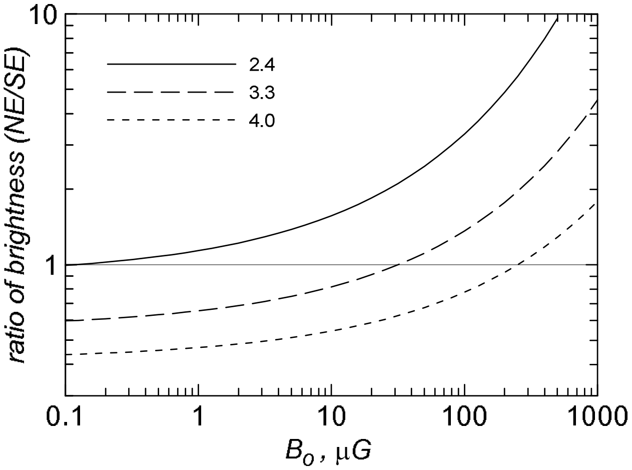

Figure 2. The ratio of $\mathcal{R}_{\rm ic}$ of IC surface brightness (at 1 TeV) in NE and SE regions of SN 1006, as it is given by Eq. (8) with observational values for $\mathcal{R}_{\rm r}$, $\mathcal{R}_{\rm x}$ and $\nu_{\rm break1}$. Calculations are done for $\alpha = 1$, $s = 2$ and three cases of MF contrast $\mathcal{R}_{\rm B}$, namely 2.4, 3.3, 4.0. In the classic model of MF inside SNR (i.e when only compression is considered which depends on the obliquity of the shock), these correspond to the aspect angles $\phi_{\rm o} = 70^{\rm o}$, $80^{\rm o}$, $90^{\rm o}$ respectively. In SN 1006, an aspect angle is $70^{\rm o}$ for a model of the uniform ISMF (Petruk et al. 2009a) or $38^{\rm o}$ for nonuniform ISMF (Bocchino et al. 2011). $\mathcal{R}_\gamma$ in the HESS data is 6.2 ± 5.4 (Acero et al. 2010).

particular, what is the range of MF strength which would result in the inversion of the γ-ray limbs in SN 1006 and therefore may be excluded?

In the radio and hard X-ray images of SN 1006, $\mathcal{R}_{\rm r} = 3.3$, $\mathcal{R}_{\rm x} = 50$. The break frequency is measured to be $\nu_{\rm break1} = 9.0 \times 10^{16}$ Hz (Miceli et al. 2009); this value corresponds to an average of the break frequencies $(5 \div 20) \times 10^{16}$ Hz measured by Katsuda et al. (2010) in a number of smaller regions. With this observables, Fig. 2 demonstrates, in a full agreement with estimation of Petruk et al. (2009c), that any MF strength $B_{\rm o} > 1\,\mu$G results in the same locations (i.e. $\mathcal{R} > 1$) of IC, radio and X-ray limbs in SN 1006, if $\mathcal{R}_{\rm B} < 3$ and α is around unity. From physical point of view, larger MF in the limbs regions (i.e. $\mathcal{R}_{\rm B} > 1$, Petruk et al. (2009a)) results in larger radiative losses of relativistic electrons emitting TeV γ-rays. The number of such electrons have therefore to be smaller there than around SE and NW regions. However, in SN 1006, $E_{\rm max}$ increases toward limbs (Petruk et al. 2011b) compensating the lack of emitting electrons due to larger MF.

This effect works in SN 1006 for the aspect angles $\phi_{\rm o} \leq 70^{\rm o}$ or for MF contrasts $\mathcal{R}_{\rm B} \leq 2.4$. If the aspect angle (or $\mathcal{R}_{\rm B}$) in SN 1006 would be larger then some ranges for $B_{\rm o}$ could be excluded by the observed fact that γ-ray limbs are at the same location as in the radio and X-ray images. For example, if $\phi_{\rm o} = 90^{\rm o}$ (Fig. 2 short-dashed line) then the only possible strength of ISMF could be greater than $\sim 100\,\mu$G.

The role of the parameter α, which determines the shape of the high-energy end of the electron spectrum, is demonstrated on Fig. 3. Namely, the cut off broader than the pure exponent (e.g. $\alpha = 0.5$, green lines) provides the same location of the bright γ-ray limbs even in case of larger differences of MF in two regions $\mathcal{R}_{\rm B}$ (or larger aspect angles, up to $90^{\rm o}$). In contrast, the thinner end of the electron spectrum is not allowed by the observed location of the γ-ray limbs ($\alpha = 2$, blue lines) and $\mathcal{R}_{\rm B} \geq 2$ because $\mathcal{R}_{\rm ic} < 1$ for such α.

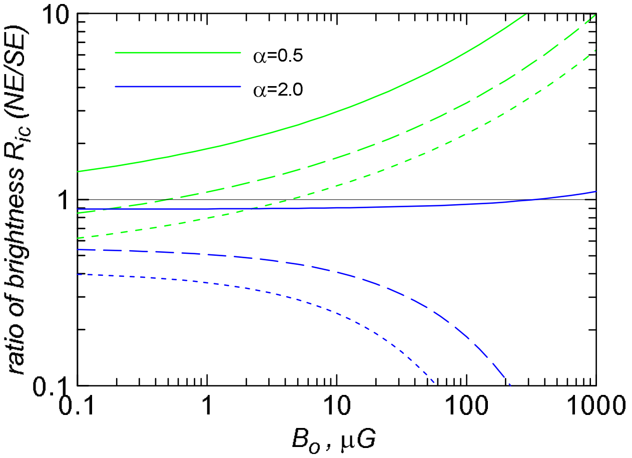

Figure 3. The same as on Fig. 2 for $\alpha = 0.5$ (green lines) and $\alpha = 2$ (blue lines).

In principle, once one has γ-ray data with high enough accuracy, namely $\mathcal{R}_\gamma$ between bright NE and faint SE regions, one can put limitations on MF from Fig. 2 and 3. However, present accuracy of the HESS azimuthal brightness profile prevents us from such an estimate. Really, the ratio of brightness between the NE (around azimuth $30^{\rm o}$) and SE (around azimuth $-60^{\rm o}$) rims in the HESS data (Fig. 6 in Acero et al. 2010) is 6.2 ± 5.4.

4 PROPERTIES OF GEV γ-RAY IMAGE OF SN 1006 AS IT COULD BE SEEN BY FERMI TELESCOPE

Eq. (7) may be used for the γ-ray image where most of emission arises from electrons with energies around cut off, $E \sim E_{\rm max}$. This is the case of TeV observations by HESS. Fermi γ-ray telescope operates in GeV γ-rays. Most of contribution to emission at these energies are from electrons with $E \ll E_{\rm max}$. Therefore, Eq. (2), which is written for $\mathcal{R}_{\rm B} = 1$, simplifies to $q_{\rm ic} \propto q_{\rm r} B^{-(s+1)/2}$ and Eq. (4) to

$$\mathcal{R}_{\rm ic,Fermi} = \mathcal{R}_{\rm r}. \tag{9}$$

Therefore, if the γ-ray emission of SN 1006 is due to the inverse-Compton process then contrast between limbs in the Fermi image should be the same as in radio. This will provide an important direct evidence about leptonic nature of γ-rays in SN 1006. If contrast between limbs in Fermi image differs from the contrast in the radio image then it should be that either MF strengths in limb locations are different or contribution to γ-rays from hadronic process is not negligible in SN 1006.

The properties of image for the former possibility, namely $\mathcal{R}_{\rm B} \neq 1$, are represented by

$$\mathcal{R}_{\rm ic,Fermi} \simeq \mathcal{R}_{\rm r} \mathcal{R}_{\rm B}^{-(s+1)/2} \tag{10}$$

instead of Eq. (8). So, having contrasts of brightness in Fermi image measured, we may directly have variations of MF strength over the SNR surface. Then this information may be used as input for the above sections providing us with measurements of the MF strength.

5 CONCLUSIONS

H.E.S.S. cooperation has reported the detection of SN 1006 at the 1% Crab flux level (Acero et al. 2010). In the SNR's image, two TeV lobes are visible coinciding with limbs in radio and X-rays (Acero et al. 2010). An application of the approach developed in Petruk et al. (2009c) to SN 1006 provides argument that such coincidence may be considered as evidence about leptonic nature of TeV γ-ray emission of this SNR. The approach uses data of radio and X-ray observations as well as considers a number of assumptions about the strength and configuration of MF.

In the present note, that approach is "inverted". Namely, we propose a new, almost model-independent methods and analytical approximations, Eqs. (7) and (8), for estimation of the MF strength which uses contrasts in the radio, X-ray and TeV γ-ray images of SNR. The methods require however a γ-ray image with high spatial resolution and accuracy, comparable to the radio and X-ray maps. Unfortunately, HESS data prevent us from determination of the MF strength; present γ-ray data limit MF in limbs to values lower than few hundred μG. We believe that future observations considerably narrow the allowed range for MF strength.

We show that the IC γ-ray limbs in SN 1006 should be in the same locations as in the radio and X-ray images for any $B_{\mathrm{o}} > 0.1\mu G$, if the aspect angle is $\leq 70^{\mathrm{o}}$ or the MF contrasts between NE and SE regions is ≤ 2.4. If actual aspect angle or MF contrast are larger then some range of B_{o} might be excluded by the fact of the same location of IC and synchrotron limbs. This is true if the high-energy end of the electron spectrum is similar to a pure exponent (i.e. for $\alpha \approx 1$). In case it is broader ($\alpha < 1$), the range of allowed aspect angles increases up to 90^{o} or R_{B} may be as large as 4 or even larger (as it could be, e.g., in case of the nonuniform ISMF). The narrower cut off ($\alpha > 1$) may be excluded in SN 1006 for $R_{\mathrm{B}} > 2$ by the observed location of the bright TeV γ-ray limbs.

The number of unknown parameters in our methods (namely, two: $\mathcal{R}_{\mathrm{B}}$ and α) may be reduced with the use of the GeV image of SN 1006 which is expecting from the Fermi γ-ray telescope. Since electrons emitting GeV γ-rays have energies smaller than the cut off, this image is not sensitive to the variation of $E_{\max}$ and, together with the radio image, may provide direct measurements of $\mathcal{R}_{\mathrm{B}}$. If the contrast of brightness between the bright limbs on the Fermi image is the same as on the radio image, this provides a direct evidence about the leptonic nature of γ-rays in SN 1006.

We would like to note that our rough upper limit is higher than available estimates of the MF strength in SN 1006. Namely, Berezhko et al. (2003, 2009) estimates the post-shock field from the width of the hard X-ray filaments as $\approx 150\,\mu$G (this is strength deduced from the thinnest filament, therefore MF is expected to be smaller in other places). Vink (2006) presents smaller estimate, $30\div40\,\mu$G. The latter value is in agreement with the strength required by the 'leptonic' model of the HESS collaboration (Acero et al. 2010) where SNR is roughly considered as uniform plasma. More detailed calculations which consider distributions of MF and emitting particles inside SN 1006, yield $32\,\mu$G for an average MF (inverse-Compton scenario for TeV γ-rays, Petruk et al. 2011b) or $150\,\mu$G for assumed uniform MF inside SNR (scenario of dominating hadronic emission in TeV γ-rays, Berezhko et al. 2009). Petruk et al. (2011b) fits the same sharpest profile as used by Berezhko et al. (2003) with $95\,\mu$G with a bit different model parameters. However, the post-shock MF in the limbs is estimated as $\leq 45\,\mu$G since most of the radial profiles of the hard X-ray brightness are thicker than in the thinnest filament (Petruk et al. 2011b).

ACKNOWLEDGMENTS

F.B. acknowledges partial support from the ASI-INAF agreement n. I/009/10/0. O.P. acknowledges partial support from the program 'Kosmomikrofizyka' (NAS of Ukraine).

REFERENCES

Acero F., et al. 2010, A&A 516, 62

Aharonian F. & Atoyan A., 1999, A&A, 351, 330

Berezhko E.G., Ellison D. C. 1999, ApJ, 526, 385

Berezhko E. G., Ksenofontov L. T., Völk H. J. 2003 A&A, 412, L11

Berezhko, E. G., Ksenofontov, L. T., Völk, H. J. 2009 A&A, 505, 169

Blasi P. 2002, Astropart. Phys, 2002, 16, 429

Blasi P. 2010, MNRAS, 402, 2807

Bocchino F., Orlando S., Miceli M., Petruk O. 2011 A&A, 531, 129

Ellison, D. C., Berezhko, E. G., & Baring, M. G. 2000, ApJ, 540, 292

Ellison, D. C., Slane, P., & Gaensler, B. M. 2001, ApJ, 563, 191

Kang H. 2011, J. Korean Astr. Soc., 44, 49

Kang, H. & Ryu, D. 2010, ApJ, 721, 886

Katsuda S., Petre R., Mori K., Reynolds S. P., Long K. S., Winkler P. F., Tsunemi H. 2010, ApJ, 723, 383

Kang, H., Ryu, D., Jones, T.W. 2009, ApJ, 695, 1273

Lazendic, J. S., Slane, P. O., Gaensler, B. M., et al. 2004, ApJ, 602, 271

Miceli M., Bocchino F., Iakubovskyi D., Orlando S., Telezhinsky I., Kirsch M. G. F., Petruk O., Dubner G., Castelletti G., 2009, A&A, 501, 239

Petruk O. 2006, A&A, 460, 375

Petruk O., Dubner G., Castelletti G., Iakubovskyi D., Kirsch M., Miceli M., Orlando S., Telezhinsky I., 2009a, MNRAS, 393, 1034

Petruk O., Beshley V., Bocchino F., Orlando S., 2009b, MNRAS, 395, 1467

Petruk O., Bocchino F., Miceli M., Dubner G., Castelletti G., Orlando S., Iakubovskyi D., Telezhinsky I., 2009c, MNRAS, 399, 157

Petruk O., Orlando S., Beshley V., Bocchino F., 2011a, MNRAS, 413, 1657

Petruk O., Beshley V., Bocchino F., Orlando S., Miceli M., 2011b, MNRAS, 413, 1643

Reynolds S. P. 1996, ApJ, 459, L13

Reynolds S. P., 1998, ApJ, 493, 375

Reynolds S., Keohane J. 1999, ApJ, 525, 368

Schure K. M., Achterberg A., Keppens R., Vink J. 2010, MNRAS, 406, 2633

Uchiyama, Y., Aharonian, F. A., & Takahashi, T. 2003, A&A, 400, 567

Vink J. 2006, Proc. The X-ray Universe 2005, Ed. A. Wilson, 319 (http://adsabs.harvard.edu/abs/2006ESASP.604..319V)

Zirakashvili V. N., Aharonian F. A., 2007, A&A, 465, 695

APPENDIX A: ROLE OF THE POSSIBLE CONCAVITY OF THE ELECTRON ENERGY SPECTRUM

The volume emissivity of the population of relativistic electrons with the energy spectrum (1) is

$$q(\nu) = \int N(E) p(\nu, E) dE \tag{A1}$$

where ν is the frequency, p is the single-electron emissivity.

In case of the synchrotron process, $p \propto BF(\nu/\nu_{\rm c})$, $\nu_{\rm c} = c_1 B E^2$, F is the special function. It is known that in the range of electron energies where the spectrum (1) do not have abrupt changes, one can use the delta-function approximation of $F(\nu/\nu_{\rm c})$ to obtain

$$q(\nu_{\rm r}) \propto K B^{(s+1-\delta s_{\rm r})/2} \tag{A2}$$

for radio band and

$$q(\nu_{\rm x}) \propto K B^{(s+1-\delta s_{\rm x})/2} \exp\left[-\left(\nu/\nu_{\rm break}\right)^{\alpha/2}\right] \tag{A3}$$

for X-rays; $\delta s_{\rm r}$ and $\delta s_{\rm x}$ corresponds to the electron energies which give maximum contribution to emission at radio and X-ray frequencies respectively. However, delta-function approximation is not adequate for the exponential part where the spectrum varies quite quickly; it is necessary to consider the full single-particle emissivity there (Reynolds 1998). We need therefore to correct (A3) respectively. An approximation

$$q(\nu_{\rm x}) \propto K B^{(s+1-\delta s_{\rm x})/2} \exp\left[-\beta_{\rm x}\left(\nu/\nu_{\rm break}\right)^{0.364\beta_{\alpha{\rm x}}}\right] \tag{A4}$$

accurately restores the numerical convolution of the electron distribution (1) with the full single-particle synchrotron emissivity (expressions for $\beta_{\rm x}$ and $\beta_{\alpha{\rm x}}$ are given in Sect. 2). Substitution of K from (A2) into (A4) yields

$$q_{\rm x} \propto q_{\rm r} B^{-(\delta s_{\rm x}-\delta s_{\rm r})/2} \exp\left(-\beta_{\rm x}\left(\frac{\nu_{\rm x}}{\nu_{\rm break}}\right)^{0.364\beta_{\alpha{\rm x}}}\right). \tag{A5}$$

Comparison of this expression with Eq. (5) (where $\delta s = 0$) reveals the role of the eventual concave shape of the electron energy spectrum represented in Eq. (1) by $\delta s(E)$.

In a similar fashion, the inverse-Compton emissivity of γ-rays with energy 1 TeV may be represented by the approximation

$$q(\nu_{\rm ic}) \propto K \exp\left[-\beta_{\rm ic}\beta_{\alpha{\rm ic}}\left(c_1 B/\nu_{\rm break}\right)^{0.375\beta_{\alpha{\rm x}}}\right] \tag{A6}$$

(expressions for $\beta_{\rm ic}$ and $\beta_{\alpha{\rm ic}}$ are given in Sect. 2). Substitution of K from (A2) into (A6) yields (cf. with Eq. 2)

$$q_{\rm ic} \propto q_{\rm r} B^{-(s+1)/2} B^{\delta s_{\rm r}/2} \exp\left(-\beta_{\rm ic}\beta_{\alpha{\rm ic}}\left(\frac{c_1 B}{\nu_{\rm break}}\right)^{0.375\beta_{\alpha{\rm x}}}\right). \tag{A7}$$

It is clear now that δs does not appear directly in the expressions for ratios of the IC γ-ray and synchrotron X-ray emissivities, $\mathcal{R}_{\rm ic} = q_{\rm ic1}/q_{\rm ic2}$ and $\mathcal{R}_{\rm x} = q_{\rm x1}/q_{\rm x2}$, of the two regions with the same MF strength B. Namely, the expressions are the same as (4) and (6). However, if the electron energy spectrum hardens toward $E_{\rm max}$ then one has to use $s + \delta s_{\rm x}$ and $s + \delta s_{\rm ic}$ instead of s in $\beta_{\rm x}$ and $\beta_{\rm ic}$. Nevertheless, ξ in Eq. (7) is almost insensitive to values of s in the range $1.8 \div 2.5$. Thus, possible hardening of the electron spectrum toward high energies does not affect results of the Sect. 2.

Let us consider the role of δs in ratios $\mathcal{R}_{\rm ic}$ and $\mathcal{R}_{\rm x}$ for the two regions with different MF strengths, $B_1 \neq B_2$. In this case, as it follows from (A7), the right-hand side of Eq. (8) should be multiplied by $\mathcal{R}_{\rm B}^{\delta s_{\rm r}/2}$. Electrons emitting radio waves at 1.5 MHz in MF $B \sim 10 \div 100\,\mu$G have energies $\sim 100\,$MeV. The function δs varies from 0 at $E \simeq m_{\rm e}c^2 = 0.5\,$MeV to ≤ 0.5 around $E \simeq E_{\rm max} \sim 10\,$TeV. Around $E \sim 100\,$MeV, it reaches the value $\delta s \sim 0.1$. Therefore, $\mathcal{R}_{\rm B}^{\delta s_{\rm r}/2} \approx 1$ in wide range of $\mathcal{R}_{\rm B}$. Thus, also in this case our results are negligibly affected by the eventual concavity of the electron energy spectrum.